J|A|C|S
ARTICLES

Published on Web 06/13/2008

# Indirect, Reversible High-Density Hydrogen Storage in Compact Metal Ammine Salts

Rasmus Z. Sørensen,[†] Jens S. Hummelshøj,[‡,§] Asbjørn Klerke,[†] Jacob Birke Reves,[†] Tejs Vegge,[§] Jens K. Nørskov,[‡] and Claus H. Christensen*[,†]

*Center for Sustainable and Green Chemistry, Department of Chemistry, Building 206, Technical University of Denmark, DK-2800 Kgs. Lyngby, Denmark, Center for Atomic-scale Materials Design, Department of Physics, Building 310, Technical University of Denmark, DK-2800 Kgs. Lyngby, Denmark, and Materials Research Department, Risø National Laboratory for Sustainable Energy, NanoDTU, Building 228, Technical University of Denmark, DK-4000 Roskilde, Denmark*

Received September 14, 2007; E-mail: chc@kemi.dtu.dk

Ⓦ **This paper contains enhanced objects available on the Internet at http://pubs.acs.org/jacs.**

***Abstract:*** The indirect hydrogen storage capabilities of $Mg(NH_3)_6Cl_2$, $Ca(NH_3)_8Cl_2$, $Mn(NH_3)_6Cl_2$, and $Ni(NH_3)_6Cl_2$ are investigated. All four metal ammine chlorides can be compacted to solid tablets with densities of at least 95% of the crystal density. This gives very high indirect hydrogen densities both gravimetrically and volumetrically. Upon heating, $NH_3$ is released from the salts, and by employing an appropriate catalyst, $H_2$ can be released corresponding to up to 9.78 wt % H and 0.116 kg H/L for the $Ca(NH_3)_8Cl_2$ salt. The $NH_3$ release from all four salts is investigated using temperature-programmed desorption employing different heating rates. The desorption is found mainly to be limited by heat transfer, indicating that the desorption kinetics are extremely fast for all steps. During desorption from solid tablets of $Mg(NH_3)_6Cl_2$, $Mn(NH_3)_6Cl_2$, and $Ni(NH_3)_6Cl_2$, nanoporous structures develop, which facilitates desorption from the interior of large, compact tablets. Density functional theory calculations reproduce trends in desorption enthalpies for the systems studied, and a mechanism in which individual chains of the ammines are released from the surface of the crystal is proposed to explain the fast absorption/desorption processes.

## Introduction

The rising concern over dwindling resources and the environmental impact of burning fossil fuels has generated interest in using hydrogen as an alternative energy carrier. Significant challenges remain in the development of economically viable solutions for production, storage, and use of hydrogen as an energy carrier.[1–6]

Widespread use of hydrogen as a fuel is limited by the lack of safe and efficient systems for its storage.[7] The large deviation from ideality observed upon compression of hydrogen to high pressures, combined with the low condensing point and low density even in the liquid state, has limited the use of conventional storage systems, and a plethora of strategies for direct storage of hydrogen have been proposed.[8–14] Clearly, direct hydrogen storage methods will involve the lowest possible number of chemical transformations, and thereby minimize the inherent losses associated with multistep chemical reactions, but in practice there are still a large number of challenges to be dealt with before such large-scale direct hydrogen storage is technically and economically feasible. This has led to increased interest in indirect storage of hydrogen, e.g., in the form of methanol, ethanol, ammonia, urea, or guanidine.[15–18]

[†] Center for Sustainable and Green Chemistry, Department of Chemistry.
[‡] Center for Atomic-scale Materials Design, Department of Physics.
[§] Materials Research Department, Risø National Laboratory for Sustainable Energy.

(1) Dresselhaus, M.; Crabtree, G.; Buchanan, M. Basic Research Needs for the Hydrogen Economy; U.S. Department of Energy: Washington, DC, 2003. (available online at http://www.sc.doe.gov/bes/hydrogen.pdf).
(2) Crabtree, G.; Dresselhaus, M.; Buchanan, M. *Phys. Today* **2004**, *57, 12*, 39–44.
(3) Kennedy, D. *Science* **2004**, *305*, 917.
(4) Turner, J. A. *Science* **2004**, *305*, 972–974.
(5) Wu, W.; Kawamoto, K.; Kuramochi, H. *J. Mater. Cycles Waste Manag.* **2006**, *8*, 70–77.
(6) Avci, A. K.; Önsan, Z. I.; Trimm, D. L. *Top. Catal.* **2003**, *22*, 359–367.
(7) Takimoto, M.; Hou, Z. *Nature* **2006**, *443*, 400–401.
(8) Zütel, A. *Naturwissenschaften* **2004**, *91*, 157–172.
(9) Cheng, P.; Xiong, Z.; Lou, J.; Lin, J.; Tan, K. L. *Nature* **2002**, *420*, 302–304.
(10) Bououdina, M.; Grant, D.; Walker, G. *Int. J. Hydrogen Energy* **2006**, *31*, 177–182.
(11) Stephens, F. H.; Baker, R. T.; Matus, M. H.; Grant, D. J.; Dixon, D. A. *Angew. Chem., Int. Ed.* **2006**, *46*, 746–749.
(12) Bogdanoviæ, B.; Felderhoff, M.; Pommerin, A.; Schüthe, F.; Spielkamp, N. *Adv. Mater.* **2006**, *18*, 1198–1201.
(13) Latroche, M.; Surblé, S.; Serre, C.; Mellot-Draznieks, C.; Llewellyn, P. L.; Lee, J.-H.; Chang, J.-S.; Jhung, S. H.; Férey, G. *Angew. Chem., Int. Ed.* **2006**, *45*, 8227–8231.
(14) Welch, G. C.; Juan, R. R. S.; Masuda, J. D.; Stephan, D. W. *Science* **2006**, *314*, 1124–1126.
(15) Metkemeijer, R.; Achard, P. *Int. J. Hydrogen Energy* **1994**, *19*, 535–542.
(16) Thomas, G.; Parks, G. Potential Roles of Ammonia in a Hydrogen Economy; U.S. Department of Energy: Washington, DC, 2006. (available online at http://hydrogen.energy.gov/pdfs/nh3_paper.pdf).
(17) Christensen, C. H.; Johannessen, T.; Sørensen, R. Z.; Nørskov, J. K. *Catal. Today* **2006**, *111*, 140–144.


**10.1021/ja076762c CCC: $40.75** 

***Table 1.*** Mass and Volume of 10 kg of Hydrogen Stored Reversibly by Six Different Methods[a]

| $Mg(NH_3)_6Cl_2$ | $H_2$ (liquid) | $Mg_2NiH_4$ | $LaNi_5H_6$ | $NaAlH_4$ | $H_2$ (g, 200 bar) |
|---|---|---|---|---|---|
| 91.4 L | 141.2 L | 252.6 L | 276.9 L | 380.9 L | 714.2 L |
| 109 kg | 10 kg | 392 kg | 730 kg | 286 kg | 10 kg |

[a] All data are based on the best-obtained reversible densities reported in the literature without considering the space occupied by the container.[26–32]

Molecular ammonia contains 17.8 wt % hydrogen and can be used directly as a fuel in internal combustion engines[19] or in solid oxide fuel cells,[20] but it can also be catalytically converted to hydrogen and nitrogen at temperatures below 650 K[21–23] in high yields. The production of ammonia from hydrogen and nitrogen using natural gas as the feedstock has been optimized in the Haber−Bosch process,[24] which is among the largest catalytic processes currently in industrial operation.[25] Commercially, ammonia is transported as a liquid at a pressure around 16 bar, achieved by addition of nitrogen, but for distribution to consumers the safety of this solution is a concern.[26]

In Table 1, the practically obtainable hydrogen storage density of a selection of the more promising direct hydrogen storage approaches is compared to the results of a recently published method of hydrogen storage in the ammine complex $Mg(NH_3)_6Cl_2$. From Table 1, it is evident that reversible storage of 10 kg of H in a compact and convenient way is not a trivial task. Since the comparison indicates that the hexaammine magnesium salt is a promising candidate for hydrogen storage, it is interesting to explore the hydrogen storage potential for a broader range of metal ammine salts. Recently, metal ammines have also been proposed for ammonia storage in connection with vehicular $DeNO_x$ systems,[33] giving an extra incentive for studying these materials in more detail.

Here, $Ca(NH_3)_8Cl_2$, $Mn(NH_3)_6Cl_2$, and $Ni(NH_3)_6Cl_2$ are investigated and compared with $Mg(NH_3)_6Cl_2$ as hydrogen/ammonia storage materials to demonstrate that the family of metal ammine salts, in fact, represents a large number of compounds that can potentially be used for reversible, indirect hydrogen storage. Furthermore, the investigated metal ammine complexes are found to exhibit facile ammonia release kinetics.

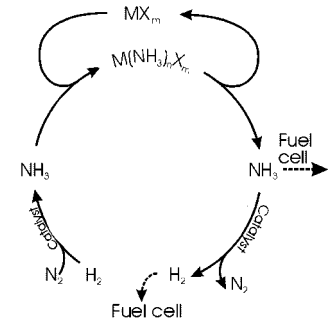


***Figure 1.*** Principle of hydrogen storage in metal ammine salts of the general formula $M(NH_3)_nX_m$.

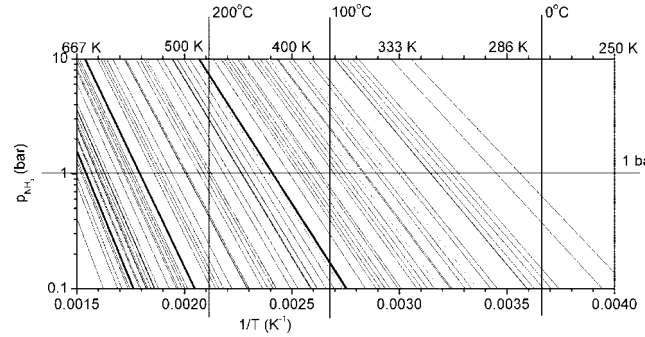


***Figure 2.*** Van't Hoff plot showing the equilibrium pressure of ammonia over 90 metal ammine halides of the general formula $M(NH_3)_nX_2$.[34] The complete list of complexes is given as Supporting Information.

The general principle of storing hydrogen in metal ammine complexes is shown in Figure 1. The absorption of ammonia is exothermic (negative absorption enthalpy) for all salts. Thus, the release is necessarily endothermic and must require the same amount of energy as is released during the absorption. The equilibrium vapor pressures can be determined by the van't Hoff relationship given as eq 1, from which it is seen that the safer the storage material (low vapor pressure at ambient temperature), the more energy required for releasing $NH_3$ at a given pressure.

$$\ln(p) = -\frac{\Delta H_{\mathrm{des}}}{RT} + \frac{\Delta S_{\mathrm{des}}}{R} \qquad (1)$$

The possibility for choosing a metal ammine salt with the desired thermodynamic properties is illustrated in Figure 2.

Compared to hydrides and alanates with comparable storage pressures, the pressure change with temperature is larger for metal ammines. This is because the ammine salts generally have higher entropies of desorption than those of metal hydrides. Thus, it is evident from the van't Hoff relationship that metal complexes also have higher enthalpies of desorption than hydrides with similar vapor pressures at a given temperature.

The formation of metal ammine complexes and the thermodynamics of ammonia desorption from these have been thoroughly described in the early chemical literature. From these literature data, it is possible to find general trends for the $NH_3$

(18) Van Vechten, J. A. Presented at the 2007 APS March Meeting, Denver, CO;; American Physical Society: College Park, MD, 2007; Abstract S39.00010.
(20) Fournier, G. G. M.; Cumming, I. W.; Hellgardt, K. *J. Power Sources* **2006**, *162*, 198–206.
(19) Steele, R. B. *Chemtech* **1999**, (August), 28.
(21) Raróg-Pilecka, W.; Szmigiel, D.; Kowalczyk, Z.; Jodzis, S.; Zielinski, J. *J. Catal.* **2003**, *218*, 465–469.
(22) Li, X.-K.; Ji, W.-J.; Zhao, J.; Wang, S.-J.; Au, C.-T. *J. Catal.* **2005**, *236*, 181–189.
(23) Boisen, A.; Dahl, S.; Nørskov, J. K.; Christensen, C. H. *J. Catal.* **2005**, *230*, 309–312.
(24) Schlögl, R. *Angew. Chem., Int. Ed.* **2003**, *42*, 2004–2008.
(25) Eggmann, T. *Kirk-Othmer Encyclopedia of Chemical Technology: Ammonia*; John Wiley & Sons, Inc.: New York, 2001.
(26) Appl, M. *Ullmann's Encyclopedia of Industrial Chemistry: Ammonia*; Wiley-VCH Verlag GmbH & Co. KGaA: Weinheim, 2007.
(27) Mosher, D.; Tang, X.; Arsenault, S. High Density Hydrogen Storage System Demonstration Using $NaAlH_4$ Based Complex Hydrides. FY 2006 Annual Progress Report, DOE Hydrogen Program; U.S. Department of Energy: Washington, DC, 2006; pp 281−284. (available online at http://www.hydrogen.energy.gov/pdfs/progress06/iv_a_1_mosher.pdf).
(28) Liu, X.; Zhu, Y.; Li, L. *Int. J. Hydrogen Energy* **2007**, *32*, 2455–2460.
(29) Nomura, K.; Fujiwara, S.; Hayakawa, H.; Akiba, E.; Ishido, Y.; Ono, S. *Journal of the Less-Common Metals* **1991**, *169*, 9–17.
(30) Suissa, E.; Jacob, I.; Hadari, Z. *J. Less-Common Metals* **1984**, *104*, 287–295.
(31) El-Osairy, M. A.; el-Osery, I. A.; Metwally, A. M.; Hassan, M. A. *Int. J. Hydrogen Energy* **1993**, *18*, 517–524.
(32) Laidler, K. J.; Meiser, J. H. *Physical Chemistry*, 3rd ed.; Houghton Mifflin Co.: New York, 1999.
(33) Elmøe, T. D.; Sørensen, R. Z.; Quaade, U.; Christensen, C. H.; Nørskov, J. K.; Johannessen, T. *Chem. Eng. Sci.* **2006**, *61*, 2618–2625.
(34) Biltz, W.; Messerknecht, C. *Z. Anorg. Allg. Chem.* **1923**, *129*, 161–175.

desorption properties of metal ammine halides.[35–37] The most general trend in these original data is that the desorption enthalpy of ammonia increases from chloride through bromide to iodide. The data available for fluorides indicate that fluoride does indeed follow the same trend, but, in fact, only a few metal ammine fluorides have been investigated in detail.[35,37–39] The effect of the metal cation is not as clear, but some trends can be seen. For the alkali and alkaline earth metals, the enthalpy of desorption decreases down through the groups,[37,38] and for the transition metals, the enthalpy of desorption increases slightly when moving from left to right in the Periodic Table, i.e., from manganese to nickel in oxidation state 2+.[37]

For a metal ammine complex to be considered useful as an indirect hydrogen storage material, it needs to desorb ammonia in a relatively narrow temperature range around or above ambient temperature. For the storage to be safe, the ammonia vapor pressure should preferably be below 1 bar at ambient temperature. Possibly, somewhat higher pressures could be handled appropriately in practical systems. However, with such materials, leaks would represent a significant hazard. At the same time, 1 bar of ammonia pressure should preferably be reached below 650 K for all desorption steps to avoid desorption of ammonia becoming too energy intensive. This is so because the ammonia decomposition reaction is best conducted above 650 K, where a sufficiently high rate can be achieved and simultaneously a sufficiently low equilibrium ammonia concentration is reached. Moreover, the gravimetric and volumetric hydrogen density of the chosen metal ammine salt(s) should clearly be as high as possible. This criterion obviously favors light cations and anions such as alkali metals and fluorides. These are, however, impractical because the alkali metals do not bind ammonia sufficiently well at ambient temperature according to the above criteria, and the fluorides are usually toxic and can form hydrofluoric acid when they are heated to desorb the ammonia.[39]

So far, the only metal ammine complex which has been investigated in any detail as an indirect hydrogen storage material is $Mg(NH_3)_6Cl_2$.[40] $Mg(NH_3)_6Cl_2$ was chosen initially because it has a vapor pressure of only 2.2 mbar at 300 K, and additionally $MgCl_2$ is both widely available and nontoxic. However, other salts can similarly bind ammonia to form interesting indirect hydrogen storage materials. For one, $CaCl_2$ binds eight ammonia molecules to form $Ca(NH_3)_8Cl_2$ at 300 K and 1 bar of $NH_3$. This gives an even higher indirect hydrogen storage density than that achieved in $Mg(NH_3)_6Cl_2$ on both a mass and volume basis, but it also results in an equilibrium ammonia pressure of 0.77 bar at 300 K. In $Ca(NH_3)_8Cl_2$, only six of the $NH_3$ molecules are coordinated directly to calcium. The last two are more freely bound in the crystalline structure.[41] $MnCl_2$ and $NiCl_2$ coordinate ammonia to form $Mn(NH_3)_6Cl_2$ and $Ni(NH_3)_6Cl_2$, respectively. Both of these have higher molar masses than $Mg(NH_3)_6Cl_2$, but as their crystal densities are also higher,[42] the volumetric hydrogen contents are essentially the same as in $Mg(NH)_6Cl_2$. The temperatures at which the equilibrium vapor pressure is 1 bar for the first desorption step in the four different complexes are 305 ($Ca(NH_3)_8Cl_2$), 358 ($Mn(NH_3)_6Cl_2$), 413 ($Mg(NH_3)_6Cl_2$), and 449 K ($Ni(NH_3)_6Cl_2$).[43] The theoretical storage capacities of the metal ammine complexes are given in Table 2, and desorption enthalpies for the individual desorption steps are reported separately in Table 3.

***Table 2.*** Indirect Hydrogen Storage Capacity of Four Metal Ammine Salts

| | $\rho$,[a] g/cm$^3$ | gravimetric H, wt % H | volumetric H, kg H/L |
|---|---|---|---|
| $Mg(NH_3)_6Cl_2$ | 1.25 | 9.19 | 0.115 |
| $Ca(NH_3)_8Cl_2$ | 1.19 | 9.78 | 0.116 |
| $Mn(NH_3)_6Cl_2$ | 1.41 | 7.96 | 0.112 |
| $Ni(NH_3)_6Cl_2$ | 1.53 | 7.83 | 0.119 |

[a] Crystal densities.[42]

***Table 3.*** Ammonia Desorption Enthalpies for Each Desorption Step for Four Different Metal Ammine Complexes[43]

| $Mg(NH_3)_nCl_2$ | | $Ca(NH_3)_nCl_2$ | | $Mn(NH_3)_nCl_2$ | | $Ni(NH_3)_nCl_2$ | |
|---|---|---|---|---|---|---|---|
| $n$ | $\Delta H_{des}$, kJ/mol | $n$ | $\Delta H_{des}$, kJ/mol | $n$ | $\Delta H_{des}$, kJ/mol | $n$ | $\Delta H_{des}$, kJ/mol |
| 6→2 | 55.7 | 8→4 | 41.0 | 6→2 | 47.4 | 6→2 | 59.2 |
| 2→1 | 74.9 | 4→2 | 42.3 | 2→1 | 71.0 | 2→1 | 79.5 |
| 1→0 | 87.0 | 2→1 | 63.2 | 1→0 | 84.2 | 1→0 | 89.8 |
| | | 1→0 | 69.1 | | | | |

In utilizing the present approach for indirect hydrogen storage above the gram scale, it is important that the complexes can be compacted into tablets or other shaped bodies with as little void space as possible. This was previously reported to be possible for $Mg(NH_3)_6Cl_2$, and it was found that, during desorption of ammonia from tablets of this salt, a sponge-like structure maintaining the shape of the original tablet was formed featuring a nanopore system, which facilitates desorption of ammonia from the interior of the compact material.[44,45]

The compactability, the ability to form of nanopores, and the kinetics of ammonia desorption are investigated in this study for $Ca(NH_3)_8Cl_2$, $Mn(NH_3)_6Cl_2$, and $Ni(NH_3)_6Cl_2$, and the results are reported in the following sections.

## Experimental Methods

Commercial anhydrous salts ($CaCl_2$, Alfa Aesar, 97%; $NiCl_2$, Aldrich, 98%; $MnCl_2$, Aldrich, 98%) were transferred to the reaction vessel in a glovebox containing dry air (6−8 ppm $H_2O$) and dried at 400−500 °C in a stream of $N_2$ before use. The vessel was purged with $NH_3$ gas (Hede Nielsen, N45) and left overnight under a pressure of $NH_3$ slightly above 4 bar. $NH_3$ uptakes were determined gravimetrically. Each metal ammine halide was pressed into tablets to determine the maximal bulk density of the storage material. Tablets of the material were also subjected to measurements of pore size distributions. These were performed using nitrogen absorption and desorption measurements on a Micrometrics ASAP 2020N, with pretreatment of the samples at temperatures and pressures chosen to give the desired levels of $NH_3$ desorption.

(35) Ephraim, F. *Chem. Ber.* **1912**, *45*, 1322–1331.
(36) Biltz, W.; Hüttig, G. F. *Z. Anorg. Allg. Chem.* **1919**, *109*, 88–110.
(37) Biltz, W. *Z. Anorg. Allg. Chem.* **1923**, *130*, 93–139.
(38) Biltz, W.; Hansen, W. *Z. Anorg. Allg. Chem.* **1923**, *127*, 1–33.
(39) Patil, K. C.; Secco, E. A. *Can. J. Chem.* **1972**, *50*, 567–573.
(40) Christensen, C. H.; Sørensen, R. Z.; Johannessen, T.; Quaade, U.; Honkala, K.; Elmøe, T. D.; Køhler, R.; Nørskov, J. K. *J. Mater. Chem.* **2005**, *15*, 4106–4108.
(41) Westman, S.; Werner, P.-E.; Schuler, T.; Raldow, W. *Acta Chem. Scand.* **1981**, *35*, 467–472.
(42) Gmelin Data: 2000−2006, Gesellschaft Deutscher Chemiker licensed to MDL Information Systems GmbH; 1988−1999, Gmelin Institut für Anorganische Chemie und Grenzgebiete der Max-Planck-Gesellschaft zur Foerderung der Wissenschaften.
(43) Lepinasse, E.; Spinner, B. *Rev. Int. Froid.* **1994**, *17*, 309–321.
(44) Hummelshøj, J. S.; Sørensen, R. Z.; Kustova, M. Y.; Johannesen, T.; Nørskov, J. K.; Christensen, C. H. *J. Am. Chem. Soc.* **2006**, *128*, 16–17.
(45) Jacobsen, H. S.; Hansen, H. A.; Andreasen, J. W.; Shi, Q.; Andreasen, A.; Feidenhans'l, R.; Nielsen, M. M.; Ståhl, K.; Vegge, T. *Chem. Phys. Lett.* **2007**, *441*, 255–260.

***Table 4.*** Tablet Densities

| | $\rho_{tablet}$, g/cm$^3$ | $\rho_{crystal}$, % | volumetric H, kg H/L |
|---|---|---|---|
| $Mg(NH_3)_6Cl_2$[33] | 1.19 | 95 | 0.11 |
| $Ca(NH_3)_8Cl_2$ | 1.18 | 99 | 0.12 |
| $Mn(NH_3)_6Cl_2$ | 1.34 | 95 | 0.11 |
| $Ni(NH_3)_6Cl_2$ | 1.41 | 95 | 0.11 |

Desorption characteristics were determined by temperature-programmed desorption (TPD). Samples of 0.5 g were transferred to a closed test tube under an $NH_3$ atmosphere and heated following a desired temperature ramp. $NH_3$ was released into a carrier stream of Ar through a T-joint with a thin connection tube to maintain the $NH_3$ atmosphere over the sample. This procedure gave an $NH_3$ pressure slightly above atmospheric pressure over the ammine sample. For TPDs of $Mg(NH_3)_6Cl_2$, a sample obtained from Amminex A/S was used as received. The ammonia content in the carrier stream was determined using a Fischer-Rosemount NGA 2000 equipped with an MLT analyzer calibrated to $NH_3$ concentrations from 0.03 to 30%. Desorption rates were calculated from the ammonia content in the carrier stream and the flow of Ar, which was kept constant at 213 mL of N/min using a calibrated Brooks 5850 TR mass flow controller. For all four metal ammine salts, TPDs were obtained with heating rates of both 1 and 5 K/min.

## Results and Discussion

The behavior of the four different metal ammine chlorides during TPD is shown in Figure 3. In accordance with literature data, the trend in temperature for the first desorption peak is Ca < Mn < Mg < Ni. During TPD, $Ca(NH_3)_nCl_2$ has stable compositions with $n = 8$, 4, 2, and 1, and essentially all ammonia desorbs in the temperature range of 300−550 K. $Mn(NH_3)_nCl_2$ has stable compositions with $n = 6$, 2, and 1 and two compositions with $n < 1$. Stable structures with less than one ammonia molecule per metal atom are well known for a range of transition metal ammine salts and are therefore not unlikely, even though they have not been previously reported for $MnCl_2$. For this compound, essentially all ammonia desorbs in the temperature range of 350−675 K. TPDs of $Mg(NH_3)_nCl_2$ were reported previously, and there are stable compositions with $n = 6$, 2, and 1. Here, essentially all ammonia desorbs in the temperature range of 410−700 K. During TPD, $Ni(NH_3)_nCl_2$ shows stable compositions with $n = 6$, 2, and 1, and all ammonia desorbs in the temperature range of 440−700 K. Independently of the temperature ramp, all the TPD peaks start within a few degrees of the temperature for 1 bar equilibrium pressure calculated from literature data.[43] This and the nearly exponential rise in desorption rate with temperature indicate that desorption is equilibrium-limited, even at high desorption rates. During fast desorption, the endothermic reaction causes the sample to cool, which is evident as a small deviation from the predefined temperature ramp when the desorption peaks (data not shown). This cooling will, in effect, decrease the equilibrium vapor pressure and thereby alter the desorption rate. Hence, for large samples, heat transport to the reaction zone seems to be the main limitation on the desorption rate for all four metal ammine salts studied. This is also supported experimentally, as the shape of TPD peaks depends on the sample size (data not shown). When the sample is large, the peak is broadened and the slopes (both increasing and decreasing) are less steep. This corresponds to a larger temperature distribution inside the sample. In an earlier work, computational modeling showed heat transport to be the main limiting factor for desorption from $Mg(NH_3)_6Cl_2$.[33] The present results indicate that it is a general feature for metal ammine salts that desorption is not limited by diffusion kinetics or large activation energies, but only by thermodynamic equilibrium, and hence by heat transport to the reaction zone.

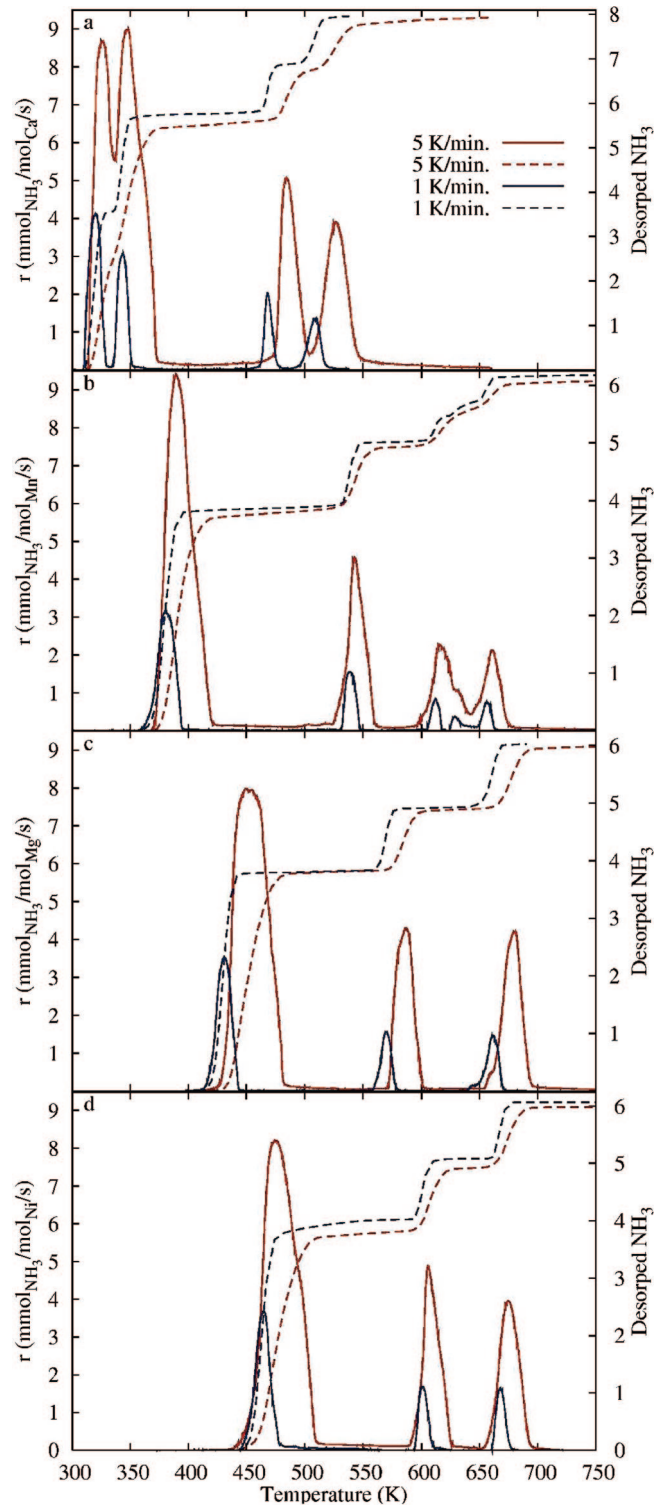


***Figure 3.*** TPDs of (a) $Ca(NH_3)_8Cl_2$, (b) $Mn(NH_3)_6Cl_2$, (c) $Mg(NH_3)_6Cl_2$, and (d) $Ni(NH_3)_6Cl_2$, with a temperature ramp of 5 K/min (red) and 1 K/min (blue). The solid lines show the desorption rate, and the dashed lines show the total amount of desorbed ammonia.

The desorption of ammonia from $Ni(NH_3)_6Cl_2$ was also examined by thermogravimetric analysis coupled with a mass spectrometer. This confirmed that the sample was maintained

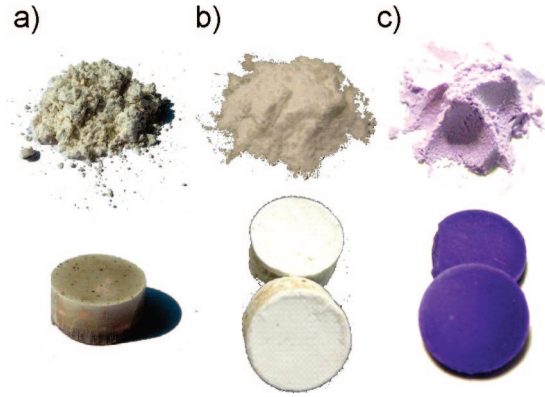


***Figure 4.*** Photos of (a) $Mn(NH_3)_6Cl_2$, (b) $Ca(NH_3)_8Cl_2$, and (c) $Ni(NH_3)_6Cl_2$ as powder and tablets.

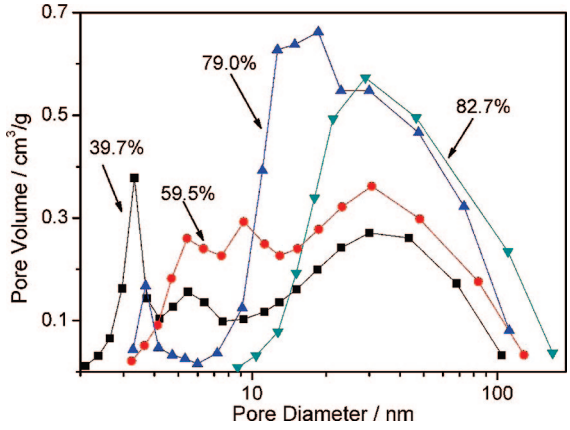


***Figure 5.*** Pore structures developed after different levels of ammonia desorption from a $Mn(NH_3)_6Cl_2$ tablet.

at complete ammonia saturation during handling and that the only gas which desorbed from the sample was ammonia.

The densities of the metal ammine chloride tablets are reported and compared to the crystal densities in Table 4. In all cases, the metal ammine halides exhibit tablet densities of at least 95% of their crystal densities. Photos of powders and tablets are given in Figure 4.

For desorption of ammonia to be facile from dense bodies of metal ammine complexes such as the present tablets, it is important that a pore structure develops through which ammonia can leave the tablet without a long diffusion path in the solid state. The development of nanopores during ammonia desorption has previously been demonstrated experimentally for $Mg(NH_3)_6Cl_2$.[44,45] Here, pore size distributions for both $Mn(NH_3)_6Cl_2$ and $Ni(NH_3)_6Cl_2$ were measured after desorption of part of the ammonia from dense tablets of these materials. Before the measurements, the samples must be evacuated at ambient temperature or higher. Therefore, some $NH_3$ necessarily desorbs before the first measurement. For $Ni(NH_3)_6Cl_2$, this loss is negligible since the vapor pressure at room temperature is very low. Hence, the porosity in the initial tablet could be characterized carefully. For $Mn(NH_3)_6Cl_2$, the initial porosity can be calculated from the tablet density in Table 4 and the crystal density in Table 2 to be 0.07 $cm^3/g$. In Figure 5, it is seen that, in the first part of desorption of $NH_3$ from $Mn(NH_3)_6Cl_2$, pores of 2−3 nm are formed along with some pores around 30−50 nm. As more and more $NH_3$ is desorbed, the smaller pores disappear while the number of larger pores increases. From 79.0% desorbed to 82.7% desorbed, something

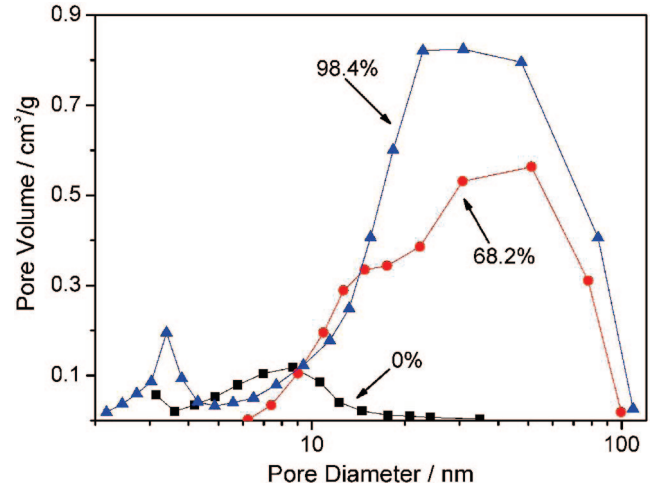


***Figure 6.*** Pore structures developed after different levels of ammonia desorption from a $Ni(NH_3)_6Cl_2$ tablet.

***Table 5.*** Pore Characteristics for $Mn(NH_3)_6Cl_2$

| $NH_3$ desorbed, % | BET area, $m^2/g$ | average pore size, nm | total pore volume, $cm^3/g$ |
|---|---|---|---|
| 0.0 | | | 0.07 |
| 39.7 | 89.6 | 10.9 | 0.308 |
| 59.5 | 84.0 | 15.6 | 0.421 |
| 79 | 91.7 | 20.3 | 0.560 |
| 82.7 | 43.3 | 35.7 | 0.507 |

***Table 6.*** Pore Characteristics for $Ni(NH_3)_6Cl_2$

| $NH_3$ desorbed, % | BET area, $m^2/g$ | average pore size, nm | total pore volume, $cm^3/g$ |
|---|---|---|---|
| 0.0 | 12.0 | 6.8 | 0.051 |
| 68.2 | 53.9 | 25.5 | 0.432 |
| 98.4 | 120.5 | 21.1 | 0.687 |

different happens. The pores of 20−30 nm diameter disappear without the number of pores in the size range 30−50 nm increasing. For $Ni(NH_3)_6Cl_2$, the data are not as detailed, but it is evident from Figure 6 that, from a relatively small pore volume with pore sizes distributed from 3 to 20 nm in the initial tablet, a larger volume of pores in the size range 10−100 nm develops as $NH_3$ desorbs. As a consequence of this development in pore structure, the average pore sizes and total pore volumes in both salts generally increase during the desorption. Table 5 lists the Brunauer−Emmett−Teller (BET) areas measured at various stages during the desorption of $NH_3$ from $Mn(NH_3)_6Cl_2$. They are almost constant until the last measurement, where a decrease is seen. For $Ni(NH_3)_6Cl_2$, however, the BET area continues to increase during the desorption process (see Table 6). As the increase in surface area makes more surface available for desorption of ammonia, this facilitates desorption of ammonia from the interior of dense bodies of the material.

**Modeling of Ammonia Desorption.** A series of periodic density functional theory (DFT) calculations, using the Dacapo planewave pseudopotential implementation,[46–48] were performed to determine this method's ability to accurately calculate ammonia desorption enthalpies for metal ammine salts, specifically $Mg(NH_3)_6Cl_2$, $Ca(NH_3)_8Cl_2$, $Mn(NH_3)_6Cl_2$, and $Ni(NH_3)_6Cl_2$. The calculations were also used to provide additional understanding of

(46) Kresse, J. *Comput. Mater. Sci.* **1996**, *6*, 15–50.
(47) Vanderbilt, D. *Phys. Rev. B* **1990**, *41*, 7892–7895.
(48) Hammer, B.; Hansen, L. B.; Norskov, J. K. *Phys. Rev. B* **1999**, *59*, 7413–7421.

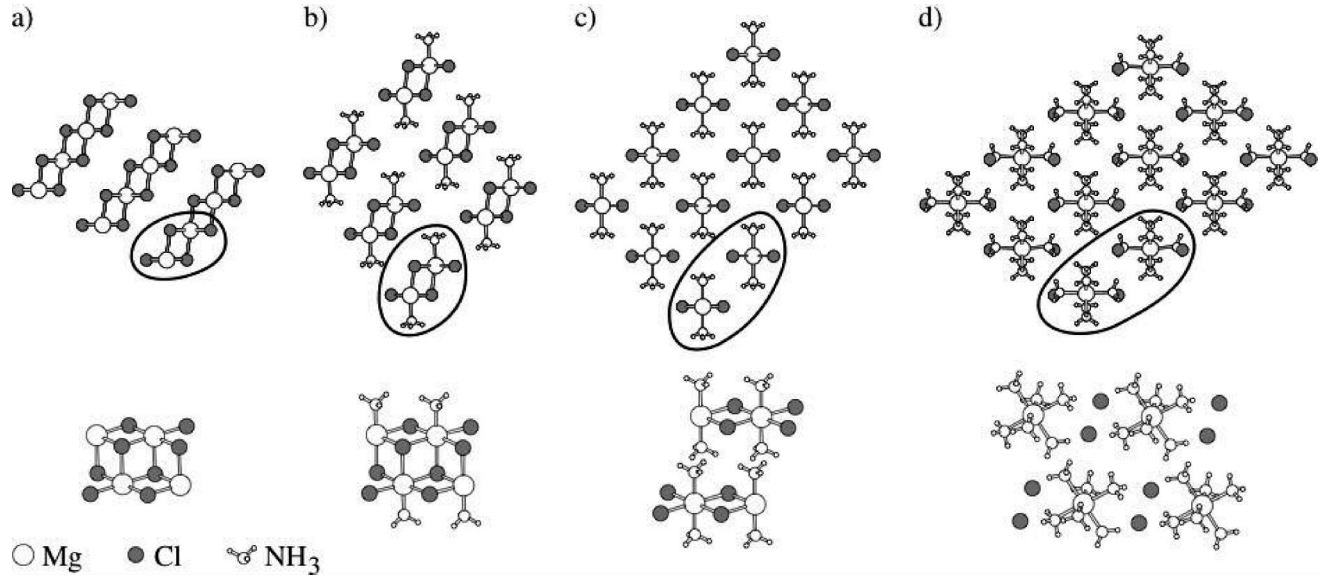


***Figure 7.*** Optimized structures found using DFT for (a) $MgCl_2$, (b) $Mg(NH_3)Cl_2$, (c) $Mg(NH_3)_2Cl_2$, and (d) $Mg(NH_3)_6Cl_2$, viewed along the chains that continue infinitely in and out of the picture. Four formula units are shown from the side, corresponding to the highlighted fragments in the end view.

the mechanistic details underlying the fast ab/desorption processes observed for these materials as described above, and finally also to predict potential electronic trends, which can be utilized in the design of novel metal ammines with optimized properties in hydrogen/ammonia storage.

**Calculation of Desorption Enthalpies.** We determine the desorption enthalpy of going from one phase to another as the difference in total energy between the most stable structures found for the two phases plus the gas-phase energy of the released ammonia molecules. The energy of an ammonia molecule in the gas phase is calculated by placing one molecule in a vacuum cube of side length 10 Å; zero-point energies are not included.

**Structures of $Mg(NH_3)_nCl_2$.** To determine the most stable structures for the different ammine phases, a rigorous search was first performed on the $Mg(NH_3)_nCl_2$ ($n = 6, 2, 1, 0$) systems based on the experimentally reported structures.[49–52] In all the structures, a central magnesium atom is coordinated octahedrally to six ligands, i.e., either chlorine atoms for $n = 0$, ammonia molecules for $n = 6$, or a combination of the two for $n = 2$ or 1, as shown in Figure 7.

For $n = 6$, the structure is of the $K_2PtCl_6$ type[49] and is traditionally described as octahedral $Mg(NH_3)_6$ complexes contained in a cubic lattice of chlorine atoms, with Mg body-centered and $NH_3$ face-centered in every second cube of chlorine atoms, but the structure can also be described as chains of $Mg(NH_3)_6Cl_2$, as seen in Figure 7d, running along the face diagonals of the cubes. In the optimized DFT structure, the experimentally observed $K_2PtCl_6$ structure is slightly distorted.

For $n = 2$, each chlorine atom is shared by two neighboring magnesium atoms in edge-sharing octahedral chains. The space group is *Cmmm*, with cell parameters $a = 8.73$ Å, $b = 8.82$ Å, and $c = 4.17$ Å somewhat larger than the experimental ones of $a = 8.18$ Å, $b = 8.21$ Å, and $c = 3.76$ Å.[50]

For $n = 1$, a chlorine atom is shared by three magnesium atoms in edge-sharing double octahedral chains. In the experimental structure found for $Ni(NH_3)Cl_2$,[51] which is believed to be isostructural with the $Mg(NH_3)Cl_2$ equivalent, the double octahedral chains have two orientations in the *I*2/*m* space group. This structure was reproduced in our calculations; however, a structure very similar to this one with respect to coordination of the H atoms, but with only one orientation of the chains, was found to have the same energy. For practical computational reasons, the simple structure as shown in Figure 7b was chosen for further calculations.

For $n = 0$, the octahedra of chlorine atoms with central magnesium atoms share half of their edges, resulting in layers of $MgCl_2$ of the $CdCl_2$ type. The space group is $R\bar{3}m$, with $a = 3.78$ Å and $c = 18.52$ Å, compared to $a = 3.64$ Å and $c = 17.67$ Å in the experiment.[52] As found in experiments,[52] the octahedra that are occupied by Mg are flattened, and the empty octahedra between the layers are elongated. The ratio of the short and the long edges of the occupied octahedra are $r = 0.92$, close to the value of $r = 0.934$ from the experiment.[52] In general, the lattice is a little expanded in the calculations due to the RPBE[48] functional used. The RPBE functional is known to overestimate lattice constants slightly. For a weakly bonded system like the one treated here, we expect to see this problem even more clearly—this is a general feature of GGA-type exchange correlation functionals. We will show in the following that this does not affect the ability of the RPBE functional to describe trends in stability of the ammines.

The interaction between individual $Mg(NH_3)_nCl_2$ chains in the respective structures can be examined quantitatively by comparing the total energy of a $Mg(NH_3)_nCl_2$ structure with the total energy of a $Mg(NH_3)_nCl_2$ chain in vacuum. This shows that the energy per Mg atom needed to move a chain of $Mg(NH_3)_nCl_2$ from the bulk to vacuum is 26, 48, and 76 kJ/mol for $n = 1$, 2, and 6, respectively. For $n = 0$, the corresponding value is 15 kJ/mol, calculated as the binding between fragments (highlighted in Figure 7a) of the $MgCl_2$ layers. The layers of $MgCl_2$ are actually slightly repulsive in this description.

To understand the nature of the interaction between the chains and layers of $Mg(NH_3)_nCl_2$, we use density difference plots, where the ground-state electron density of a given structure is subtracted from that of the individual atomic species comprising

(49) Olovsson, I. *Acta Crystallogr.* **1965**, *18*, 889–893.
(50) Leineweber, A.; Friedriszik, M. W.; Jacobs, H. *J. Solid State Chem.* **1999**, *147*, 229–234.
(51) Leineweber, A.; Jacobs, H.; Ehrenberg, H. *Z. Anorg. Allg. Chem.* **2000**, *626*, 2146–2152.
(52) Partin, M. *J. Solid State Chem.* **1991**, *95*, 176–183.

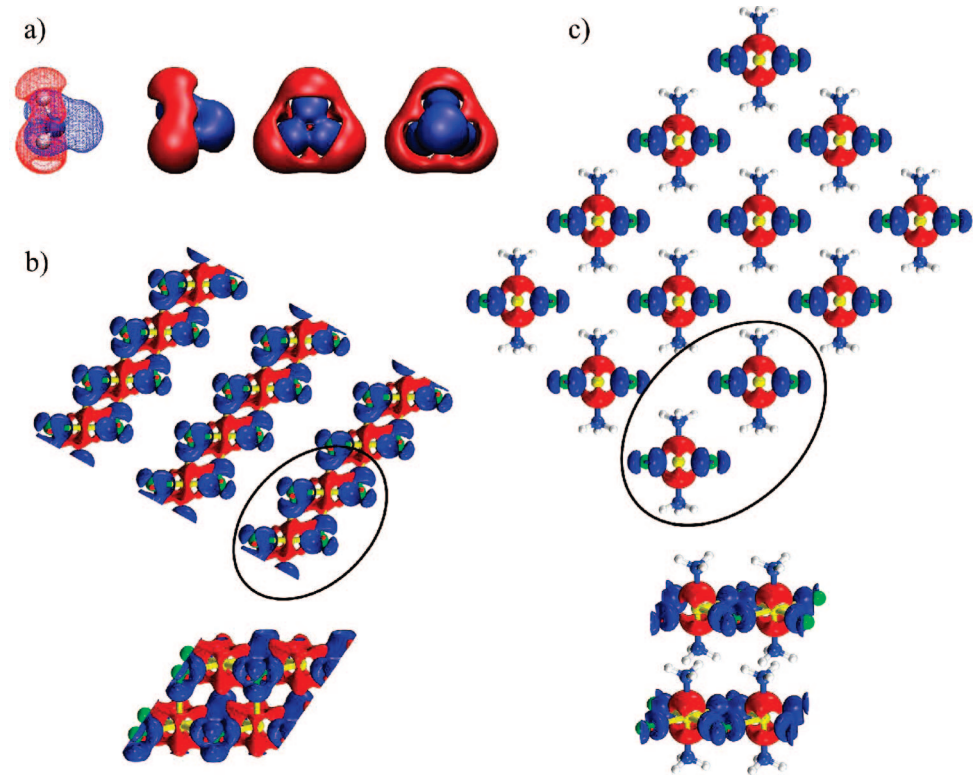


***Figure 8.*** Density difference plots of (a) a $NH_3$ molecule, (b) $MgCl_2$, and (c) Mg and Cl in $Mg(NH_3)_2Cl_2$ (yellow, Mg; green, Cl; blue, N; and white, H). Blue areas correspond to an excess of electrons or negative charge, and red indicates depletion of electrons or positive charge. In (b) and (c), four formula units are shown from the side, corresponding to the highlighted fragments in the end view.

the structure treated alone and in the same positions. This effectively shows how the electron density is redistributed, and by plotting isosurfaces of density increments and decrements, negatively and positively charged areas become visible.

Some density difference plots are shown in Figure 8, where one can see (i) the lone pair of ammonia and the positively charged hydrogen atoms (Figure 8a); (ii) how the electrons concentrate around the chlorine atoms in a $MgCl_2$ layer (Figure 8b), with the negatively charged areas protruding the layer, rendering them slightly repulsive; and (iii) the charge redistribution caused by Mg and Cl alone in the $Mg(NH_3)_2Cl_2$ structure (Figure 8c), showing how the ammonia molecules fit nicely. In general, the lone pair of ammonia connects to the positively charged areas surrounding the magnesium atoms, and the positively charged hydrogen atoms connect to the negatively charged areas near the chlorine atoms.

Thus, the chains for $n = 6$, 2, and 1 are interconnected by the electrostatic attraction between the positively charged H atoms of an ammonia molecule and the negatively charged Cl atoms (Figure 8a,c). For $n = 0$, the layers are slightly repulsive, and the real structure is therefore mainly held together by van der Waals forces, which are not accurately described in these DFT calculations.

**Structures of the Ca, Mn, and Ni Salts.** The structures found for the Mg salt were also used for the three other salts (Ca, Mn, Ni) by simply exchanging the metal atoms and letting the structures relax while scaling the unit cell size linearly until a minimum in total energy was reached.

For $Mn(NH_3)_nCl_2$ and $Ni(NH_3)_nCl_2$, this approximation is expected to be rather precise, since these salts are known to be isostructural with the magnesium analogue for $n = 6$ and 0 and for nickel with $n = 2$ as well.[49,53,54] The $Ca(NH_3)_nCl_2$ structures, on the other hand, are different and, moreover, go through $n = 8$, 4, 2, 1, and 0. However, since the experimental enthalpies for the 8→4 and 4→2 transitions are very close in energy (41 and 42 kJ/mol, respectively; see Table 3), we rely on the 6→2 reaction enthalpy of the model to provide a reasonable approximation for both of these; here, an enthalpy of 41 kJ/mol was chosen for comparison with the 6→2 reaction enthalpy of the model.

**Results I: Desorption Enthalpies from a Stable Structure Comparison.** The calculated desorption enthalpies are compared with experimental values (see Figure 9), and it is seen that the DFT model is able to quite accurately describe the trends in desorption enthalpies of the metal ammine salts studied here.

A straight line is obtained in Figure 9, but the slope is less than 1; i.e., the calculated enthalpies of desorption are too low by a certain factor. The inclusion of zero-point energies or the use of other exchange-correlation functionals only amounts to a shift of the line and cannot account for the slope being less than 1. Although the absolute numbers are not accurate, the trend is very clear, and the precision of Figure 9 is usually considered more than acceptable in a DFT study like this.[48]

**Fast Ab/Desorption Processes.** To understand the fast ab/desorption of ammonia in the metal ammine salts, we considered the structures again, but this time from the perspective of how ammonia can get in and out of these materials. We restrict the discussion to involve only the isostructural Mg, Mn, and Ni salts and focus on the magnesium salt as a representative.

As mentioned previously, clean $MgCl_2$ has a layered structure, while the structures of $Mg(NH_3)_nCl_2$ for $n = 1$, 2, and 6 consist

(53) Ferrari, A.; Bigliard, G.; Braibant, A. *Acta Crystallogr.* **1963**, *16*, 846–847.
(54) Leineweber, H. *J. Solid State Chem.* **2000**, *152*, 381–387.

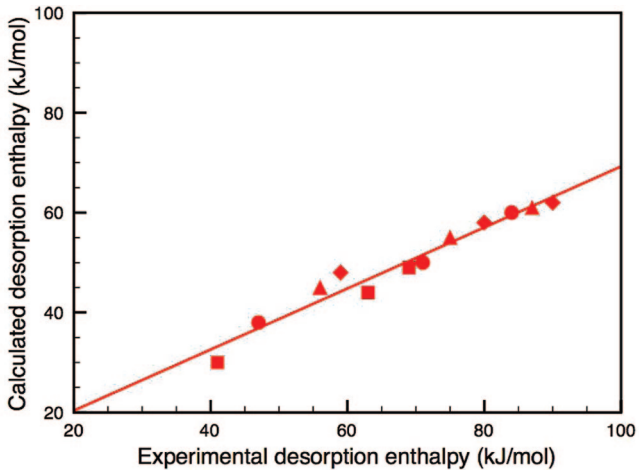


***Figure 9.*** Calculated versus experimental desorption enthalpies for the different desorption steps, 6→2, 2→1, and 1→0, of $Mg(NH_3)_6Cl_2$ (triangles), $Ca(NH_3)_8Cl_2$ (squares), $Mn(NH_3)_6Cl_2$ (circles), and $Ni(NH_3)_6Cl_2$ (diamonds) and in a comparison of stable structures. The calcium salt is approximated by model hexaammine salt $Ca(NH_3)_6Cl_2$, which follows the same desorption route as the three other salts. In this approximation, the first desorption step is representative of the first two desorption steps of the real octaammine salt, $Ca(NH_3)_8Cl_2$.

of chains (see Figure 7). Going from one phase to another, the chains/layers of the initial structure are either cleaved to absorb ammonia or recombined to desorb ammonia. For the 6→2/2→6 reactions, the chains are merely stretched/compressed (see Figure 7). In all cases, the resulting chains or layers are rearranged to produce the final structure.

The details of this cleavage and recombination and the detailed mechanism for transport of ammonia into and out of the materials are unknown, but both desorption and absorption are known from experiments to be facile.[40] We shall first consider the situation where bulk diffusion of ammonia is the dominant transport process.

**Bulk Diffusion in Metal Ammines.** The transport of ammonia out of the systems during desorption could be dominated by bulk diffusion of ammonia. Indeed, from Figure 7, it seems likely that, if ammonia desorbs by diffusing along the chains of $Mg(NH_3)_nCl_2$, the system can transform from one bulk phase directly to another in a continuous way. However, the barriers for diffusion need to be sufficiently small that no competing mechanisms become dominant.

The barriers for diffusion along the chains of $Mg(NH_3)_nCl_2$ have been calculated to be 58, 135, and 121 kJ/mol for $n = 6$, 2, and 1, respectively; this is clearly too high for $n = 2$ and 1 when compared with the experimental desorption enthalpy. If bulk diffusion of ammonia were indeed rate-limiting, one would expect the last two peaks in a TPD experiment to be broader than the first peak, which is not the case, as seen in Figure 3.

Although the bulk diffusion picture cannot be ruled out, at least for the $n = 6$ case, an alternative mechanism would be desirable. In the following, such a mechanism, which explains the fast kinetics for both the absorption and desorption processes, is proposed.

**Restructuring at the Surface.** We now consider the rather weak binding between the individual chains in $Mg(NH_3)_nCl_2$ (15, 26, 48, and 76 kJ/mol for $n = 0$, 1, 2, and 6, respectively), which allows for an alternative desorption process in which the individual chains are released from the surface to facilitate desorption or absorption of ammonia from or to the chains (see Figure 10), as investigated in the following.

Three principles underlie the proposed mechanism for understanding the dynamics of ammonia absorption and desorption: (a) it is energetically preferred for Mg to retain a six-fold coordination to the ligands (either Cl or $NH_3$), (b) chains are released from the surface to facilitate desorption or absorption, and (c) reactions involving a minimal number of chains are expected to be faster.

When a chain is released from the hexammine (Figure 10a), it releases four of its six $NH_3$ molecules per Mg and transforms into a diammine chain, thus maintaining the energetically preferred six-fold coordination of the Mg atoms (four Cl's substitute the released $NH_3$). If the hexammine chain were to release more than four $NH_3$ molecules directly, it would require the expectedly slower combination of two or more chains to keep the Mg atoms fully coordinated. The formed diammine chains will subsequently arrange into the bulk structure of $Mg(NH_3)_2Cl_2$.

As the temperature is further increased, chains break off from the diammine structure (Figure 10b). For this desorption reaction, a minimum of two chains must combine to release (half their) $NH_3$ molecules, in order to maintain the six-fold Mg coordination. The resulting monoammine chains later rearrange into the bulk structure of $Mg(NH_3)Cl_2$.

Similarly, for the monoammine structure (Figure 10c), chains combine in pairs to give $Mg(NH_3)_{0.5}Cl_2$ chains. This combination of chains to release $NH_3$ and form chains of lower ammonia content can, in principle, continue until all the ammonia is desorbed and the layered structure of $MgCl_2$ is formed. The intermediate $n < 1$ chains are, in general, not expected not to be stable, and therefore not detected in the experiments, except for $Mn(NH_3)_nCl_2$, which finds a stable arrangement of the $Mn(NH_3)_{0.5}Cl_2$ chains (see Figure 3b).

For absorption the picture is reversed, and the chains/layers are cleaved instead of combined (Figure 10d−f).

**Results II: A New Scheme for Calculating Desorption Enthalpies.** We have presented a model for the detailed mechanism behind desorption and absorption processes in metal amine salts, and we now return to the modeling of desorption enthalpies. In the alternative mechanism, the system does not transform directly from one stable structure to the next during desorption. Instead, it goes through an intermediate state where chains of the final phase are free and uncoordinated. These free chains could combine sufficiently fast into the final structure to make it reasonable to compare the energies of the stable structures, as done in Figure 8. However, it is also interesting to model the desorption enthalpies under the assumption that the free chains are sufficiently long-lived to be detected experimentally. In that case, the relevant energy to calculate is the difference between the initial ammine in its stable bulk form and the final ammine as a chain in vacuum. For the 1→0 transition, the relevant free chains are the $Mg(NH_3)_{0.5}Cl_2$ chains, as shown in Figure 10c.

This can easily be done in the DFT calculations, and the results of this scheme applied to all four salts are again compared with apparent experimental desorption enthalpies and shown in Figure 11.

Although the straight line in Figure 11 has a slope of 1, it does not confirm the mechanism presented in Figure 10, nor does it prove that desorption in the TPD experiments is not equilibrated. The slope of less than 1 in Figure 9 could very well be due to limitations in the calculations. However, it does provide a valid way to predict desorption enthalpies using DFT, which appears to be more precise than comparing the energies of the stable structures. More importantly, the mechanism which, as mentioned, is also compatible with the equilibrium situation

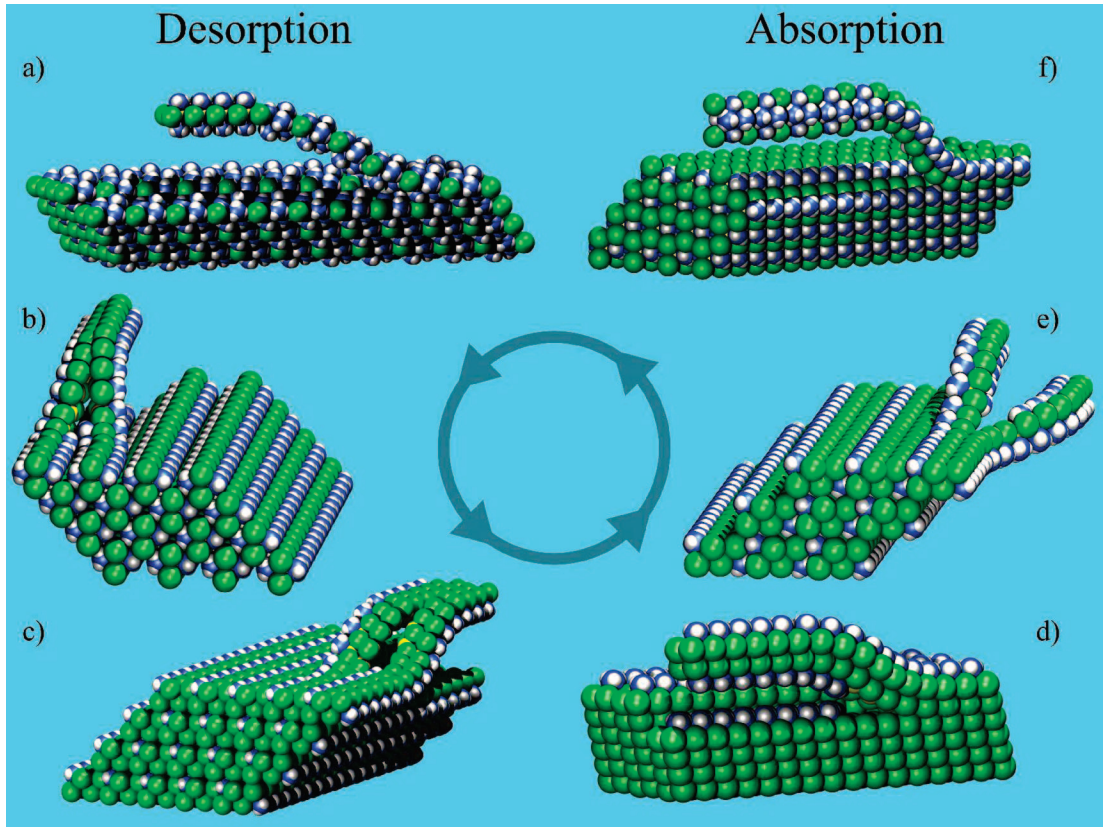


***Figure 10.*** Proposed mechanism for desorption and absorption of ammonia in $Mg(NH_3)_nCl_2$, $Mn(NH_3)_nCl_2$, and $Ni(NH_3)_nCl_2$.

Ⓦ Animations illustrating front and side views of the desorption of ammonia from modeling studies are available.

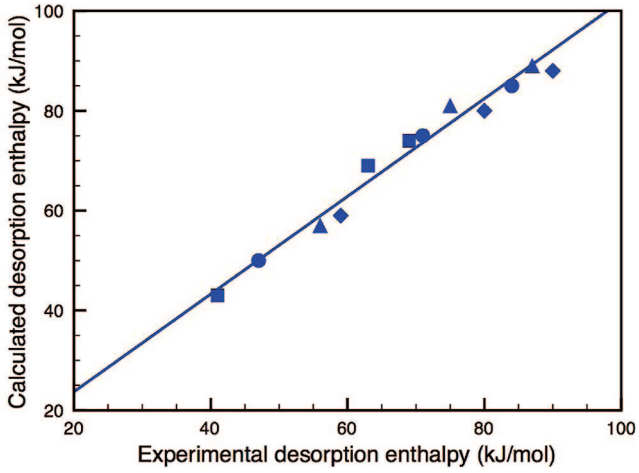


***Figure 11.*** Calculated versus apparent experimental desorption enthalpies for the different desorption steps of $Mg(NH_3)_6Cl_2$ (triangles), $Ca(NH_3)_8Cl_2$ (squares), $Mn(NH_3)_6Cl_2$ (circles), and $Ni(NH_3)_6Cl_2$ (diamonds) for the proposed mechanism in Figure 10.

explains why desorption and absorption can happen fast in all the steps of the ab/desorption processes.

## Conclusion

It is demonstrated that metal ammine complexes can be utilized as reversible, indirect hydrogen storage materials. The desorption of ammonia from $Ca(NH_3)_8Cl_2$, $Mn(NH_3)_6Cl_2$, and $Ni(NH_3)_6Cl_2$ is shown to be controlled mainly by thermodynamic equilibrium and heat transfer, as previously shown for $Mg(NH_3)_6Cl_2$. It is shown that the metal ammine complexes can be compacted to tablets with densities very close to the crystal densities and still maintain the same desorption properties. This is due to the development of nanopores in the tablets during desorption of ammonia. The nanopores facilitate diffusion of ammonia through the dense tablets.

DFT calculations are shown to reproduce accurately the trends in desorption enthalpies for all the systems studied. On the basis of extensive DFT calculations, we propose a mechanism for absorption and desorption of ammonia from metal ammine salts in which chains of the ammines are released from the surface of the crystal to explain the fast ab/desorption processes observed experimentally.

**Acknowledgment.** The authors thank Marina Y. Kustova and Mo Hongling Sønnichsen for experimental assistance and Amminex A/S for providing $Mg(NH_3)_6Cl_2$. The Danish National Research Foundation sponsors the Center for Sustainable and Green Chemistry. Lundbeck Foundation sponsors the Center for Atomic-scale Materials Design. The project is also supported by The Danish Council for Strategic Research (project no. 2104-05-0016) and the European Commission DG Research (contracts SES6-2006-51827/NESSHy and MRTN-CT-2006-032474/HYDROGEN).

**Supporting Information Available:** Table of thermodynamic properties of 90 metal ammine complexes. This information is available free of charge via the Internet at http://pubs.acs.org.

JA076762C